CELL BIOLOGY

The cohesin-associated protein Pds5A governs the meiotic spindle assembly via deubiquitination of Kif5B in oocytes

Yu Zhang[1,2], Jie Bai[2], Bo Xiong[1]*

Chromosome cohesion mediated by cohesin complex and its associated proteins is required for accurate chromosome segregation and genomic stability in mitosis. However, because of the distinct operation mechanisms, many proteins might exert different functions during meiosis in germ cells. Here, we document that cohesin-associated protein precocious dissociation of sisters 5A (Pds5A) plays a noncanonical role in the meiotic spindle assembly during oocyte maturation independent of its cohesion function. Pds5A distributes on the spindle fibers in oocytes at both metaphase I and metaphase II stages. Morpholino-based depletion or genetic ablation of Pds5A all lead to defects in spindle organization, chromosome euploidy and meiotic progression in oocytes and thus compromising the female fertility. Mechanistically, Pds5A recruits deubiquitinase ubiquitin-specific protease 14 to the spindle apparatus for stabilization of kinesin family member 5B, regulating the spindle elongation. Collectively, our findings unveil that cohesin-associated protein Pds5A can be used as a spindle regulator during oocyte meiosis.

INTRODUCTION

Chromosome cohesion is an essential cellular process that ensures the linkage between replicated sister chromatids from S phase until the onset of anaphase in many eukaryotic organisms (*1*). This cohesion allows the proper attachment of sister chromatids to spindle microtubules, hence playing a central role in the faithful segregation of chromosomes (*2*). By genetic and biochemical means, cohesin has been identified as a chromosomal multiprotein complex to form a ring structure that is indispensable for the establishment and maintenance of cohesion (*3*, *4*). Cohesin is made up of four subunits—Smc1, Smc3, an α-kleisin subunit-Mcd1/Scc1 (mitosis)/Rec8 (meiosis), and Scc3 (*5*). In addition, several accessory proteins take regulatory parts in timely loading, establishment, maintenance, and removal of cohesin complex from the chromatin (*6*). Among them, the dynamic association of cohesin with chromatin depends on a cohesin-regulatory complex formed by precocious dissociation of sisters 5 (Pds5), sororin, and Wapl in vertebrate cells (*7*). Sororin and Wapl compete to bind to a specific site on Pds5. From S phase to G_2 phase during cell cycle, Pds5 complexes with sororin to maintain the sister chromatid cohesion. In the mitotic prophase, however, Wapl displaces sororin, which is phosphorylated by kinases to form Pds5-Wapl complex, thus dislodging cohesin from chromosome arms (*8*).

Pds5 proteins contain more than 20 HEAT repeats (each consists of two α helices linked by a short loop), forming two clusters separated by a helical insert domain. Multiple HEAT repeats form extended superhelical structures and can function as scaffolds to facilitate the assembly of other molecular components (*9*, *10*). HEAT repeats correspond to tandemly arranged curlicue-like structures that appear to serve as flexible scaffolding on which other components can assemble. Pds5 appears to be a large scaffold protein having numerous, possibly similar or even uniform, sites for binding specific globular domains of other proteins. In mitotic cells, the HEAT-repeat structures of Pds5 would serve as a platform for multiple protein-protein interactions, either with cohesin subunits or with other chromosomal proteins involved in DNA repair and chromosome structure (*9*, *11*–*13*).

Notably, vertebrates have two paralogs of the Pds5 protein, Pds5A and Pds5B, which have common and unique roles in the cell growth and development (*14*, *15*). In humans, PDS5A and PDS5B share approximately 70% sequence identity in the N terminus and less than 30% identity in the C terminus, indicating that the C-terminal sequence might determine their specific functions (*7*). Except the overlapping role in the sister chromatid cohesion, PDS5A and PDS5B also exert redundant functions in the replication fork protection, chromosome folding, and the length of axial elements and telomere integrity (*16*–*18*). On the contrary, they have nonredundant roles in the gene expression and mitotic cell cycle (*14*, *15*).

Meiosis is a specialized form of cell division that involves one round of DNA replication and two rounds of chromosome segregation (*19*). In contrast to mitosis, meiosis I is unique and occurs only in germ cells to separate homologous chromosomes; meiosis II is more similar to a mitotic division, separating sister chromatids (*20*). Thus, meiosis has different regulation and mechanisms with mitosis in numerous aspects. During meiosis, it has been reported that Pds5 regulates homolog synapsis, chromosome axis length, and crossover frequency in yeast (*21*–*24*). Also, Pds5 proteins are essential for the axial element length and telomere integrity in mouse spermatocytes (*18*). However, the precise functions of Pds5 proteins during female meiosis are still largely unknown.

In the present study, we uncover a previously unidentified role of Pds5A as an essential modulator of spindle assembly during mammalian oocyte meiosis. In particular, we validated that Pds5A recruited a deubiquitinating enzyme (DUB) ubiquitin-specific peptidase 14 (Usp14) to stabilize the kinesin family member Kif5B for elongating spindle fibers, thereby ensuring oocyte development and female fertility.

RESULTS

Subcellular localization and protein expression patterns of Pds5A during mouse oocyte meiosis

We first of all investigated the spatial localization of Pds5A in mouse oocytes at different developmental stages during meiotic maturation by immunostaining. The immunofluorescent data displayed that

[1]College of Animal Sciences, Zhejiang University, Hangzhou 310058, China. [2]College of Animal Science and Technology, Nanjing Agricultural University, Nanjing 210095, China.
*Corresponding author. Email: xiongbo@zju.edu.cn

Pds5A was predominantly localized in the nucleus of oocytes at germinal vesicle (GV) stage. After GV breakdown (GVBD), Pds5A translocated to the growing microtubule fibers around chromosomes and then accumulated on the spindle microtubules at both metaphase I (MI) and MII stages (Fig. 1A). The spindle-like localization pattern was confirmed by costaining of Pds5A with α-tubulin (Fig. 1, A and B) and further verified by another antibody staining and expression of exogenous Pds5A-6×HA (hemagglutinin) in oocytes (fig. S1, A to D). However, Pds5 was not located in the kinetochores in oocytes as assessed by costaining with calcinosis, Raynaud phenomenon, esophageal dysmotility, sclerodactyly, and telangiectasia (CREST) (fig. S1E).

We next performed the immunoblotting analysis to examine the protein expression of Pds5A during meiotic progression by collecting oocytes at GV, GVBD, MI, and MII stages, respectively. The results showed that the protein levels of Pds5A were relatively constant throughout the in vitro maturation of mouse oocytes (Fig. 1, C and D). Collectively, these observations suggest that Pds5A might exert unexpected functions in the spindle assembly during female meiosis.

Depletion of Pds5A arrests the meiotic progression via activation of SAC in mouse oocytes

To uncover the potential role of Pds5A during mouse oocyte meiosis, gene-specific morpholino (MO) or small interfering RNA (siRNA) were applied to inhibit the protein expression and thus silence the function of Pds5A. Immunoblotting data revealed that approximately 80% of Pds5A protein was depleted in both MO and siRNA-injected oocytes (fig. S2, A to D), indicative of the high knockdown efficiency. We next observed the meiotic progression in oocytes depleted of Pds5A by monitoring the occurrence of GVBD and polar body extrusion (PBE), the indicators for G_2-M transition and completion of meiosis I. The results showed that depletion of Pds5A did not affect GVBD rate but cause the reduced PBE rate, which could be rescued by overexpression of corresponding Pds5A cRNA (Fig. 2, A to D, and figs. S2E and S3), suggesting that Pds5A is required for the completion of meiosis I instead of resumption of meiosis. We further analyzed the oocytes without PBE and found that most of them were arrested at MI stage (Fig. 2, E and F), suggesting that spindle assembly checkpoint (SAC) might be activated. As expected, the immunostaining of BubR1 and Mad2, two core components of SAC

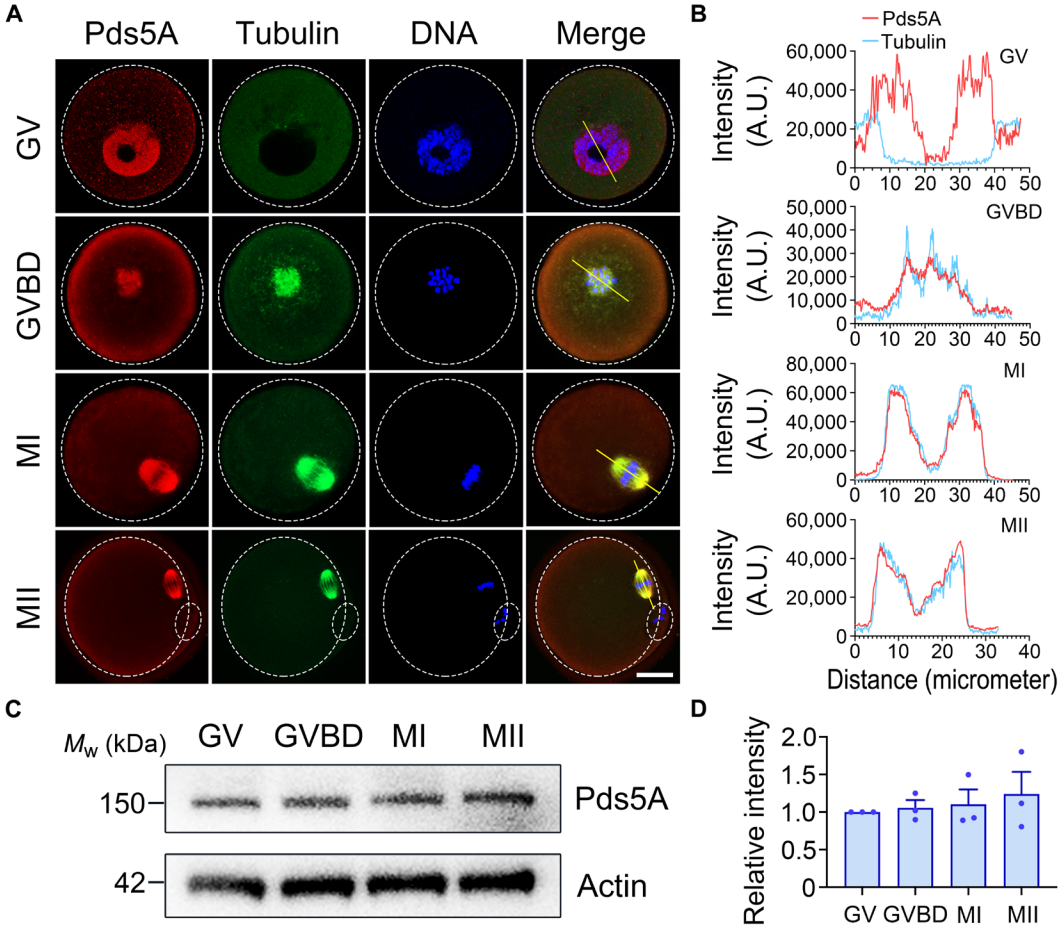

Fig. 1. Subcellular localization and protein expression patterns of Pds5A during mouse oocyte meiotic maturation. (**A**) Fluorescence images of Pds5A localization in oocytes. Mouse oocytes at different developmental stages were costained with Pds5A (Santa Cruz Biotechnology) and α-tubulin antibodies and counterstained with Hoechst 33342. Scale bar, 20 μm. (**B**) Fluorescence intensity profiles of Pds5A and α-tubulin along the yellow line in (A). (**C**) Immunoblotting analysis of Pds5A protein levels during oocyte meiosis corresponding to GV, GVBD, MI, and MII stages. The blots were probed with Pds5A (Proteintech) and β-actin antibodies, respectively. (**D**) Quantification of Pds5A protein levels during oocyte meiosis. The band intensity of Pds5A was normalized with that of β-actin. A.U., arbitrary unit.

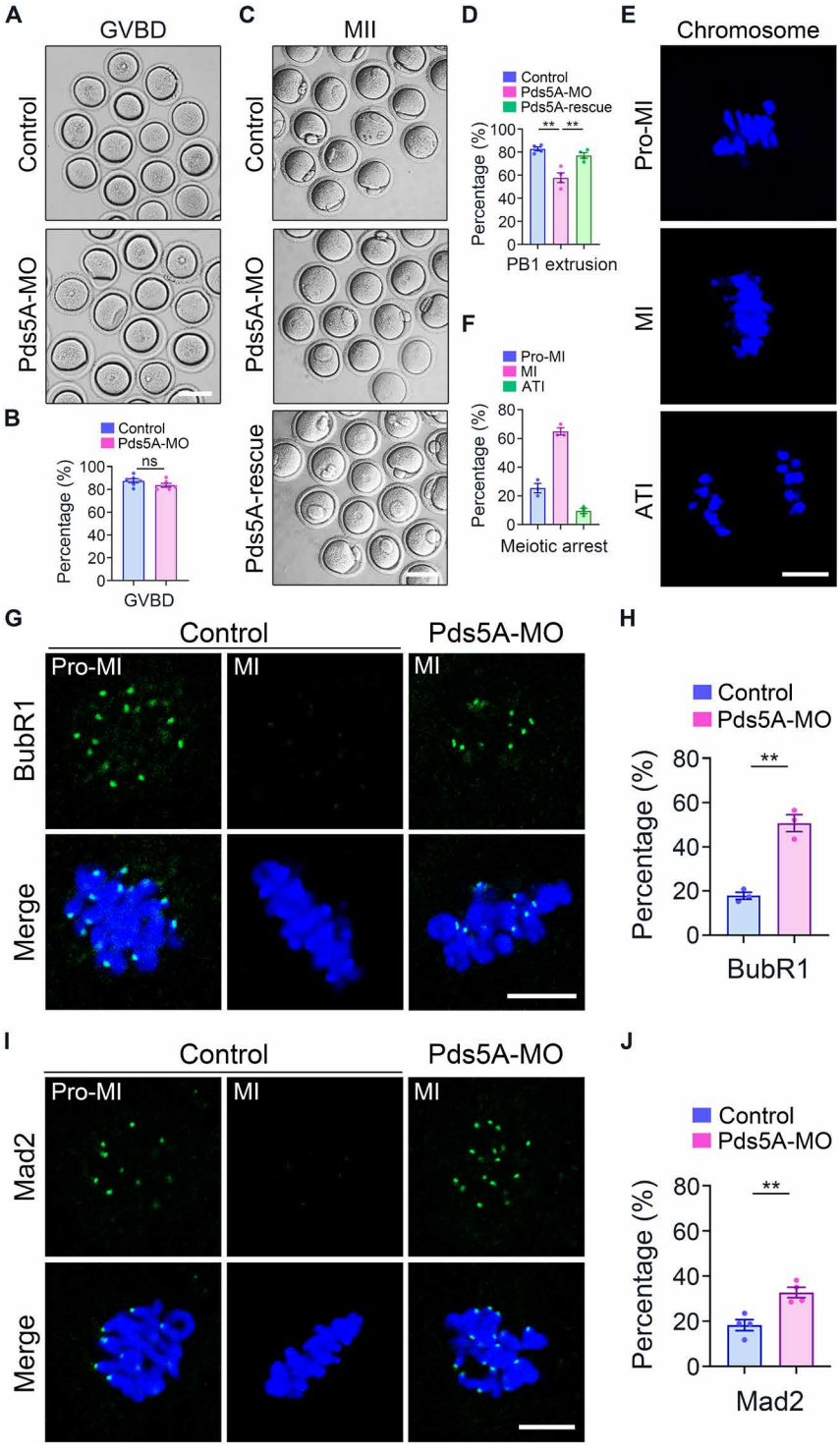

Fig. 2. Effects of Pds5A depletion on the mouse oocyte meiotic progression. (**A**) Representative images of GVBD oocytes observed at 4 hours following release from 3-isobutyl-1-metyl-xanthine in control and Pds5A-MO groups. Scale bar, 80 μm. (**B**) The rate of GVBD in control ($n = 169$) and Pds5A-MO ($n = 185$) oocytes. (**C**) Representative images of MII oocytes observed at 10 hours post-GVBD in control, Pds5A-MO, and Pds5A-rescue (Pds5A-MO + Pds5A-cRNA) groups. Scale bar, 80 μm. (**D**) The rate of PBE in control ($n = 119$), Pds5A-MO ($n = 119$), and Pds5A-rescue ($n = 113$) oocytes. (**E**) Representative images of chromosome morphology in Pds5A-MO oocytes without PB1 after maturation. Scale bar, 5 μm. (**F**) The percentage of oocytes arresting at different developmental stages in Pds5A-MO ($n = 76$) group. (**G**) Fluorescence images of BubR1 present on the chromosomes in control and Pds5A-MO oocytes at Pro-MI and MI stages. Scale bar, 5 μm. (**H**) The proportion of BubR1 presence on the chromosomes in control ($n = 73$) and Pds5A-MO ($n = 69$) oocytes at MI stage. (**I**) Fluorescence images of Mad2 present on the chromosomes in control and Pds5A-MO oocytes at Pro-MI and MI stages. Scale bar, 5 μm. (**J**) The proportion of Mad2 presence on the chromosomes in control ($n = 71$) and Pds5A-MO ($n = 86$) oocytes at MI stage. Data in (B), (D), (F), (H), and (J) were designated as mean percentage (means ± SEM) of at least three independent experiments. $^{**}P < 0.01$; ns, no significance.

complex, displayed that depletion of Pds5A led to the persistent presence of BubR1 and Mad2 at the chromosomes in MI oocytes (Fig. 2, G to J). Moreover, inhibition of Mps1 by reversine in Pds5A-depleted oocytes substantially enhanced the PBE rate (fig. S4), which indicates that the meiotic progression arrest during oocyte maturation induced by the lack of Pds5A results from the SAC activation.

Depletion of Pds5A leads to the defects in the spindle assembly during mouse oocyte meiosis

Since compromised spindle organization is one of the major causes that induce the activation of SAC, we then stained Pds5A-depleted oocytes at MI stage with α-tubulin antibody to display the spindle morphology. As shown in Fig. 3, we observed the significantly increased proportion of disorganized spindles with various types of abnormalities in Pds5A-depleted oocytes (Fig. 3, A and B). According to previous studies (*25*, *26*), we categorized them to short, elongated, multipolar, monopolar, nonpolar, and chaotic types (Fig. 3C), among of which the short spindles were dominantly present (Fig. 3D). This was further confirmed by the measurement of spindle length and width, showing the lowered length/width ratio in Pds5A-depleted oocytes (Fig. 3, E and F). Meanwhile, the increased rate of misaligned bivalents and MI plate width were also observed upon

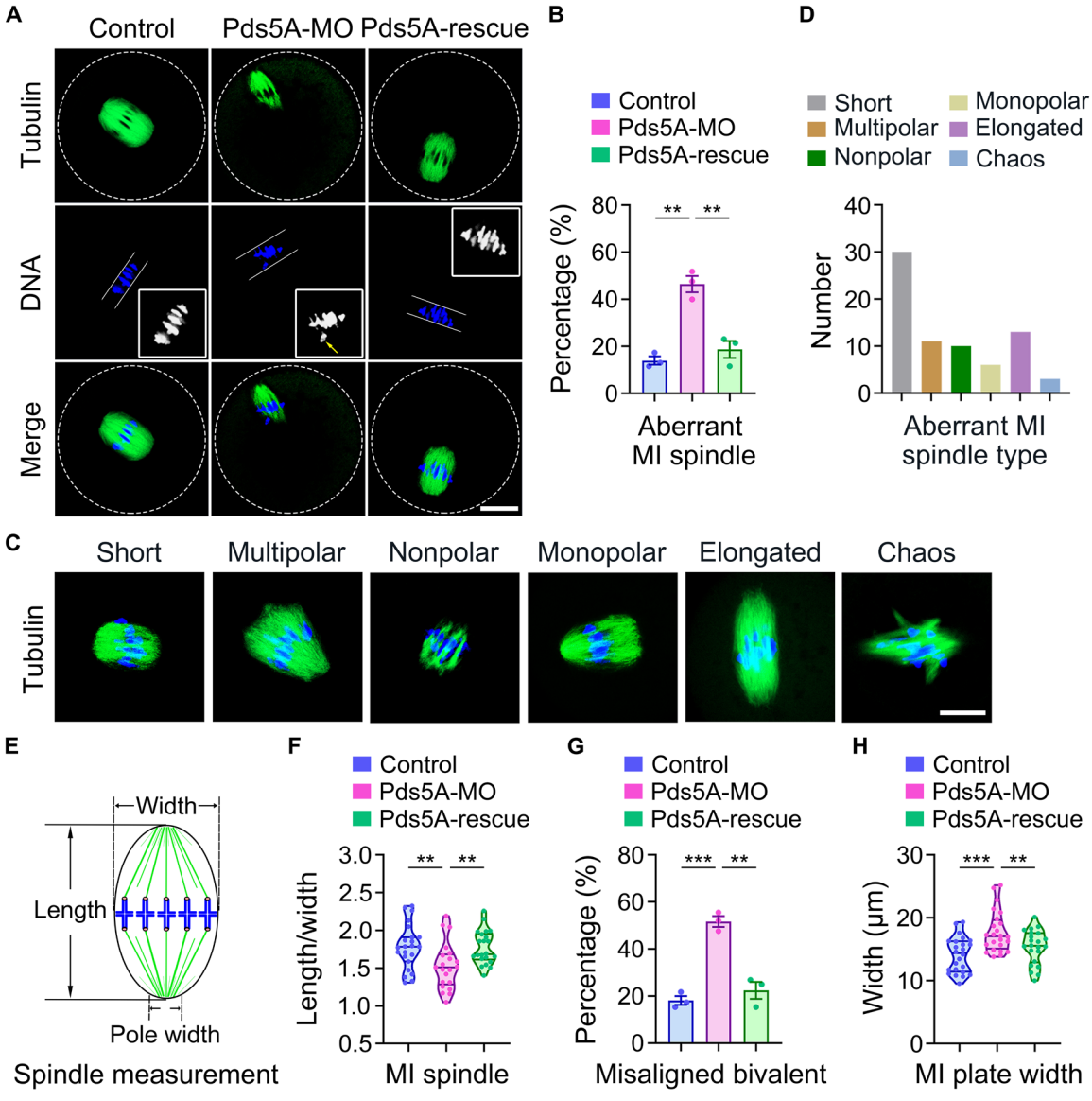

Fig. 3. Effects of Pds5A depletion on the spindle organization and chromosome alignment in mouse oocytes. (**A**) Fluorescence images of spindle morphology and chromosome alignment in control, Pds5A-MO, and Pds5A-rescue oocytes at MI stage. The yellow arrow points to the misaligned chromosomes. Scale bar, 20 μm. (**B**) The rate of abnormal spindles in control ($n = 72$), Pds5A-MO ($n = 73$), and Pds5A-rescue ($n = 80$) oocytes at MI stage. (**C**) Representative images showing different types of spindle defects observed in Pds5A-MO oocytes at MI stage. Scale bar, 10 μm. (**D**) The number of different types of spindle defects in Pds5A-MO ($n = 73$) oocytes at MI stage. (**E**) Schematic picture showing how the spindle length, width, and pole width were determined. (**F**) The ratio of spindle length to width in control ($n = 23$), Pds5A-MO ($n = 21$), and Pds5A-rescue ($n = 22$) oocytes at MI stage. (**G**) The rate of misaligned bivalents in control ($n = 72$), Pds5A-MO ($n = 73$), and Pds5A-rescue ($n = 80$) oocytes at MI stage. (**H**) Quantification of MI plate width in control ($n = 24$), Pds5A-MO ($n = 24$), and Pds5A-rescue ($n = 22$) oocytes at MI stage. Data in (B) and (G) were designated as mean percentage (means ± SEM), and (F) and (H) were designated as mean value (means ± SD) of at least three independent experiments. $^{**}P < 0.01$; $^{***}P < 0.001$.

Pds5A depletion, which was accompanied with all types of aberrant spindles (Fig. 3, A, G, and H). Of note, exogenous expression of Pds5A could alleviate the spindle/chromosome abnormalities present in Pds5A-depleted oocytes (Fig. 3, A, B, F, G, and H). Together, our data imply that Pds5A might participate in the meiotic spindle assembly through regulating the spindle elongation.

Depletion of Pds5A generates the aneuploidy in mouse oocytes

Given that abnormal spindle/chromosome structure is linked to the incorrect kinetochore-microtubule (K-M) attachment, we next tested whether this is the case after depletion of Pds5A. Costaining of α-tubulin and CREST following cold treatment of oocytes showed that most of the microtubule fibers were stably attached to the kinetochores on the chromosomes in controls (Fig. 4, A and B). However, depletion of Pds5A produced considerably more unattached kinetochores compared with the controls as cold treatment could depolymerize microtubules that did not capture kinetochores (Fig. 4, A and B). Further analysis of chromosome ploidy by chromosome spreading validated that the presence of incorrect K-M attachment in Pds5A-depleted oocytes consequently caused the elevated occurrence of aneuploidy (more than or less than 20 univalents) (Fig. 4, C and D). As expected, both defects in K-M attachment and chromosome ploidy can be relieved by expression of Pds5A cRNA in Pds5A-depleted oocytes (Fig. 4). Therefore, the above results suggest that Pds5A is required for the maintenance of euploidy during oocyte meiotic progression.

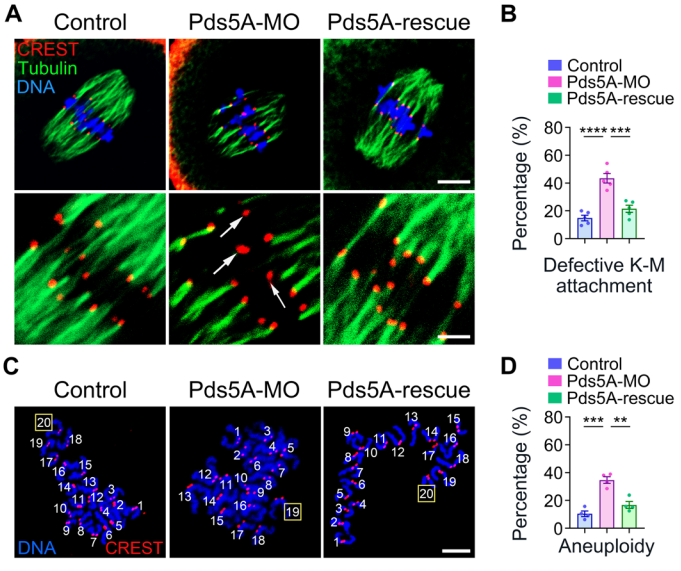

Fig. 4. Effects of Pds5A depletion on the K-M attachment and chromosome ploidy in mouse oocytes. (**A**) Fluorescence images kinetochores and microtubule fibers in control, Pds5A-MO, and Pds5A-rescue oocytes at MI stage. White arrows indicate unattached kinetochores. Scale bars, 5 and 2.5 μm. (**B**) The percentage of unattached kinetochores in control (n = 90), Pds5A-MO, (n = 125), and Pds5A-rescue (n = 103) oocytes at MI stage. (**C**) Representative images of chromosome spreads in control, Pds5A-MO, and Pds5A-rescue oocytes at MII stage. Scale bar, 8 μm. (**D**) The percentage of aneuploid oocytes at MII stage in control (n = 76), Pds5A-MO (n = 78), and Pds5A-rescue (n = 76) groups. Data in (B) and (D) were designated as mean percentage (means ± SEM) of at least three independent experiments. $^{**}P < 0.01$; $^{***}P < 0.001$; $^{****}P < 0.0001$.

Pds5A is dispensable for chromosome cohesion during mouse oocyte meiosis I

As chromosome cohesion defects can also lead to the occurrence of aneuploidy, we hence determined whether spindle/chromosome abnormalities in Pds5A-depleted oocytes resulted from the impaired cohesion. The immunostaining and fluorescence intensity quantification of Rec8, a meiotic subunit of cohesin, and Rad21, a kleisin subunit of cohesin, manifested that depletion of Pds5A did not affect the abundance of cohesin on the bivalents (fig. S5, A to D). In addition, the inter-kinetochore distance between homologs was quantified and found to be comparable in control and Pds5A-depleted oocytes (fig. S5, E and F), showing that chromosome cohesion was not influenced by Pds5A depletion. Thus, these data demonstrate that the function of Pds5A in the meiotic spindle assembly does not rely on the chromosome cohesion during oocyte meiosis I.

Heterozygous deletion of Pds5A in mice results in oocyte meiotic defects and female subfertility

To further determine the in vivo function of Pds5A during female meiosis, we generated *Pds5A* knockout mice by CRISPR-Cas9 technology (fig. S6A). As *Pds5A*-defecient mice die perinatally (*27*), we assessed their female fertility and oocyte development in heterozygous mice. Polymerase chain reaction (PCR) genotyping and immunoblotting analyses confirmed that *Pds5A* was successfully ablated in mice (fig. S6, B and C). Fertility test results showed that $Pds5A^{+/-}$ female mice produced significantly less number of pups than that of wild-type (WT) females (Fig. 5, A and B), indicating that Pds5A is essential for female fecundity. We next harvested oocytes from knockout females after superovulation and observed the reduced oocyte number, decreased oocyte maturation rate, and increased oocyte death rate in $Pds5A^{+/-}$ mice compared to WTs (Fig. 5, C to F). Moreover, we found that the dramatically higher proportions of aberrant spindles and misaligned chromosomes were present in $Pds5A^{+/-}$ oocytes (Fig. 5, G to J), consequently leading to the elevated occurrence of aneuploidy (Fig. 5, K and L). Consistently, in the oocytes in vitro cultured to MI stage, the percentages of defective spindles and misaligned bivalents significantly increased in $Pds5A^{+/-}$ group in comparison with the WT group as well (Fig. 5, M to P). In conclusion, we demonstrate that genetic deletion of Pds5A in vivo also causes the defects in spindle assembly, chromosome euploidy, and meiotic progression in oocytes, and thereby impairing the female fertility.

Identification of the downstream effector of Pds5A by MS

To decipher the molecular mechanism underlying the action of Pds5A during oocyte meiosis, we performed the immunoprecipitation coupled with mass spectrometry (MS) to identify its potential binding partners. From MS results, we noticed that Kif5B was a high score binding candidate for Pds5A (Fig. 6A). Coimmunostaining of Pds5A and Kif5B showed their colocalization on the spindle apparatus in oocytes (Fig. 6, B and C). In addition, immunoblotting analysis detected the presence of Kif5B in the immunoprecipitate pulled down by Pds5A antibody (Fig. 6D). This interaction was further verified by the reciprocal coimmunoprecipitation (co-IP) carried out using Kif5B antibody (Fig. 6E). Although Kif5B has been reported to regulate microtubule dynamics in mitotic cells (*28*, *29*), whether this is the case in oocytes has not been determined yet. Our immunostaining data validated that both endogenous and exogenous Kif5B

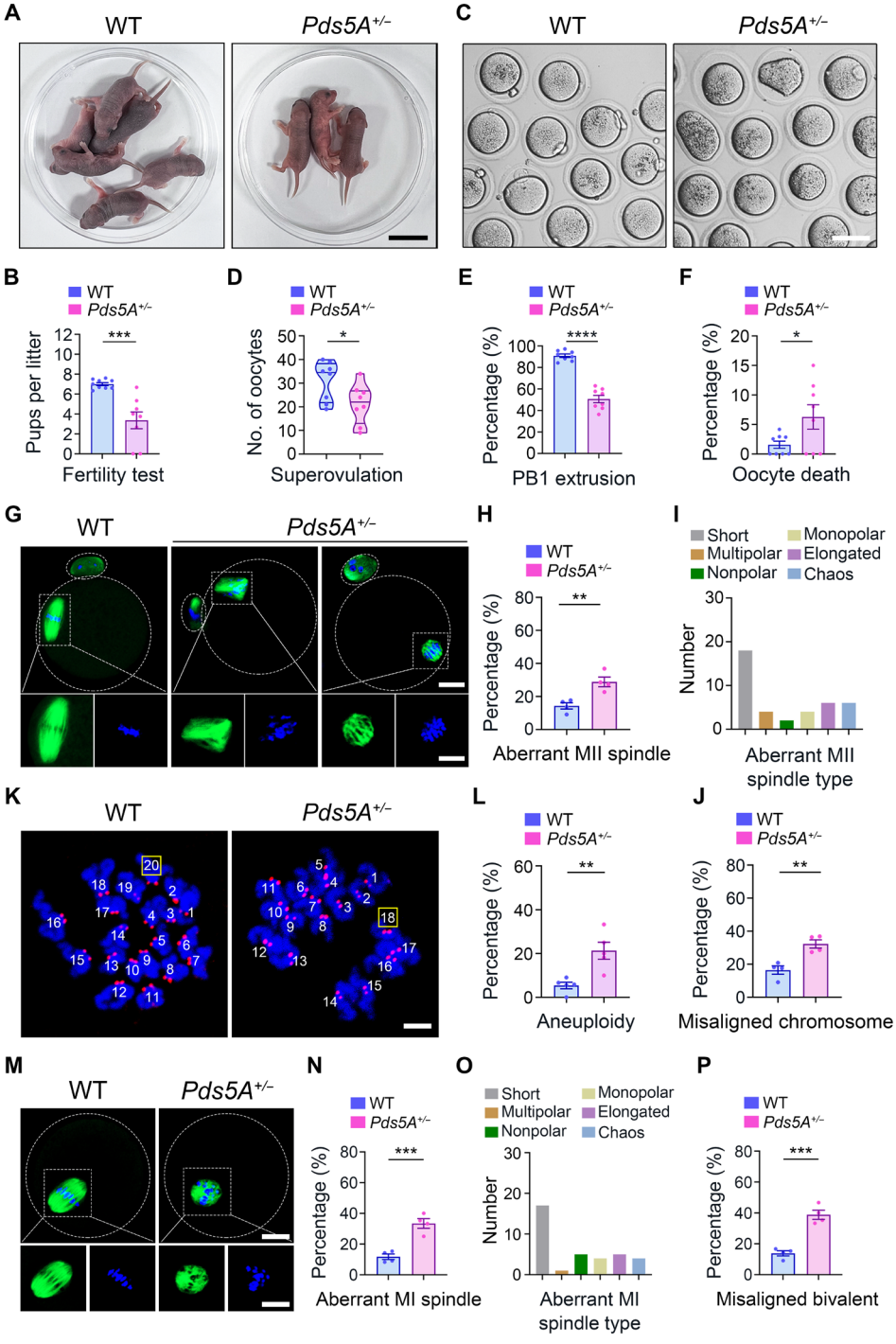

Fig. 5. The oocyte maturation and female fertility in *Pds5A*$^{+/-}$ mice. (**A**) Representative images of pups from WT and *Pds5A*$^{+/-}$ female mice. Scale bar, 1 cm. (**B**) The average number of pups per litter from WT ($n = 9$) and *Pds5A*$^{+/-}$ ($n = 8$) female mice. (**C**) Representative images of superovulated oocytes from WT and *Pds5A*$^{+/-}$ female mice. Scale bar, 80 μm. (**D** to **F**) The number, PBE rate, and death rate of superovulated oocytes in WT ($n = 248$) and *Pds5A*$^{+/-}$ ($n = 173$) groups. (**G**) Fluorescence images of spindles and chromosomes in WT and *Pds5A*$^{+/-}$ superovulated oocytes. Scale bars, 20 and 10 μm. (**H**) The rate of abnormal spindles in WT ($n = 85$) and *Pds5A*$^{+/-}$ ($n = 84$) superovulated oocytes. (**I**) The number of different defective spindles in *Pds5A*$^{+/-}$ ($n = 40$) superovulated oocytes. (**J**) The rate of misaligned chromosomes in WT ($n = 85$) and *Pds5A*$^{+/-}$ ($n = 84$) superovulated oocytes. (**K**) Representative images of chromosome spreads in WT and *Pds5A*$^{+/-}$ superovulated oocytes. Scale bar, 10 μm. (**L**) The percentage of aneuploid oocytes in WT ($n = 84$) and *Pds5A*$^{+/-}$ ($n = 57$) groups. (**M**) Fluorescence images of spindles and chromosomes in WT and *Pds5A*$^{+/-}$ MI oocytes. Scale bar, 20 μm. (**N**) The rate of abnormal spindles in WT ($n = 100$) and *Pds5A*$^{+/-}$ ($n = 118$) MI oocytes. (**O**) The number of different defective spindles in *Pds5A*$^{+/-}$ ($n = 36$) MI oocytes. (**P**) The rate of misaligned bivalents in WT ($n = 100$) and *Pds5A*$^{+/-}$ ($n = 118$) MI oocytes. Data in (B) and (D) were designated as means ± SD, and (E), (F), (H), (J), (L), (N), and (P) were designated as means ± SEM of at least three independent experiments. *$P < 0.05$; **$P < 0.01$; ***$P < 0.001$; ****$P < 0.0001$.

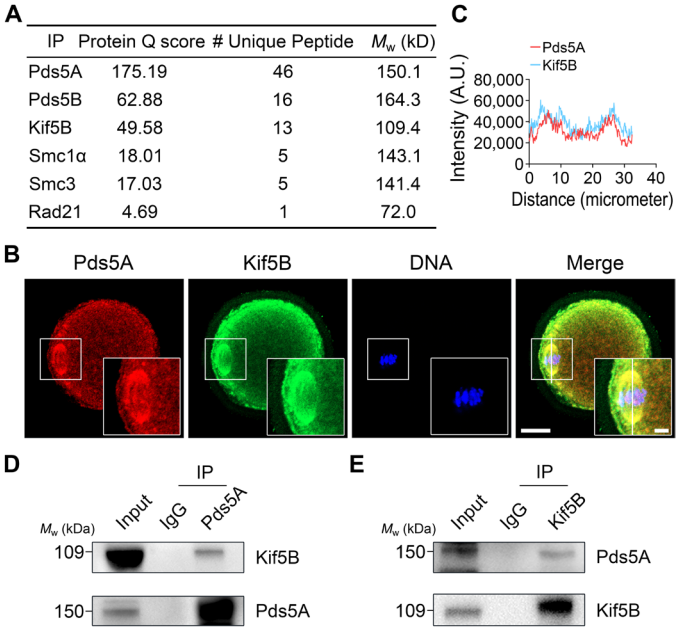

Fig. 6. Identification of binding partners of Pds5A. (**A**) Representative binding candidates of Pds5A as shown in MS data. (**B**) Costaining of Pds5A and Kif5B in oocytes at MI stage. Scale bars, 20 and 5 μm. (**C**) Fluorescence intensity profiles of Pds5A and Kif5B along the white line. (**D**) Co-IP of Pds5A and Kif5B as precipitated with Pds5A antibody. The blots of precipitates were probed with Kif5B and Pds5A antibodies, respectively. (**E**) Co-IP of Pds5A and Kif5B as precipitated with Kif5B antibody. The blots of precipitates were probed with Pds5A and Kif5B antibodies, respectively.

exhibited the spindle-like localization in mouse oocytes (fig. S7, A and B). Gene-targeted siRNA microinjection obtained a high knockdown efficiency of Kif5B in oocytes as assessed by immunoblotting (fig. S7, C and D), and depletion of Kif5B had no effect on the occurrence of GVBD (fig. S7E). However, depletion of Kif5B dramatically reduced the oocyte maturation rate and caused abnormal spindle/chromosome structure, especially the short spindles, as shown in Pds5A-depleted oocytes (fig. S7, F to L). These observations suggest that Kif5B might mediate the role of Pds5A in the meiotic spindle assembly. To confirm it, we expressed exogenous Kif5B-6×Myc protein in Pds5A-depleted oocytes. The results validated that the expression of exogenous Kif5B attenuated the meiotic defects observed in Pds5A-depleted oocytes, including decreased PBE rate, disorganized spindle/chromosome structure, and high incidence of aneuploidy (fig. S8). Together, our observations corroborate that the involvement of Pds5A in the meiotic spindle assembly is mediated by Kif5B.

Pds5A recruits Usp14 to spindle fibers for stabilization of Kif5B in mouse oocytes

To gain insights into how Pds5A affects Kif5B behavior, we examined the protein expression and localization of Kif5B in Pds5A-depleted oocytes. As assessed by immunoblotting and immunostaining analyses, depletion of Pds5A did not change the Kif5B localization pattern but dramatically reduced its protein abundance on the spindle apparatus, and this reduction could be rescued by the restoration of Pds5A levels via expression of exogenous Pds5A (Fig. 7, A to C), indicating that Pds5A is required for stability of Kif5B in oocytes. Further investigation showed that mRNA levels were not altered in Pds5A-depleted oocytes (Fig. 7D). However, MG-132 treatment increased the Kif5B protein levels in Pds5A-depleted oocytes, revealing that Pds5A regulated Kif5B stability through proteasome-mediated degradation (Fig. 7E). Intriguingly, when we revisited the MS data, we found that many DUBs were the potential binding proteins for Pds5A, including Usp9X, Usp14, Usp5, Usp7, Usp10, Usp39, Usp33, Usp47, and Usp24 (Fig. 7F). We thus proposed that DUBs might mediate the stabilization of Kif5B by Pds5A. To verify it, we firstly used the inhibitors of DUBs to determine which DUB is responsible for the stability of Kif5B. Treatment of mouse oocytes with PR-619, a broad-spectrum DUB inhibitor, substantially down-regulated Kif5B levels (Fig. 7G), suggesting that Kif5B protein is indeed modified by the DUBs. We next applied the inhibitors of Usp9X, Usp14, Usp5, and Usp7 to treat oocytes and found that treatment with IU1, the Usp14 inhibitor, remarkably decreased the Kif5B protein levels (Fig. 7, H to K), demonstrating that Usp14 is the dominant DUB for the deubiquitylation of Kif5B in oocytes. This result was further verified in oocytes depleted of Usp14 using the gene-targeting siRNA (fig. S9). Of note, co-IP experiment confirmed the interaction between Pds5A and Usp14 (Fig. 7L). We also observed that Pds5A colocalized with Usp14 on the spindle apparatus as shown by the immunostaining (Fig. 7, M and N), and depletion of Pds5A decreased the abundance of Usp14 on the spindle fibers but not whole protein levels in oocytes (Fig. 7, O to Q), implying that Pds5A is essential for the recruitment of Usp14 to the spindle apparatus for deubiquitylation of Kif5B.

The function of Pds5A during oocyte meiosis is conserved in pigs

To clarify whether the unique role of Pds5A found in mouse oocytes is conserved in other mammals, we used porcine oocytes as a model for the verification. Depletion of Pds5A in porcine oocytes by microinjection of porcine Pds5A-targeting siRNA showed a remarkable decrease of PBE rate in comparison with the controls (fig. S10, A and B). Meanwhile, depletion of Pds5A caused spindle/chromosome abnormalities and reduced protein levels of Kif5B in porcine oocytes as observed in mouse oocytes (fig. S10, C to F). Hence, these observations indicate that the meiotic function of Pds5A in oocytes is highly conserved between mice and pigs.

DISCUSSION

At the early stage of mitosis, Pds5 proteins associate with sororin to maintain the sister chromatid cohesion by stabilizing cohesin complex. By prophase, binding of Wapl to Pds5 displaces sororin, activating cohesin release from chromosome arms to allow for the separation of sister chromatids (*30*). However, during oocyte meiosis I, homologous chromosomes pair up and undergo recombination at prophase I and then segregate at anaphase I (*31*). The release of cohesin from bivalent arms requires separase instead of Pds5-Wapl complex (*32*). Thus, Pds5 proteins might exert additional functions during oocyte meiotic maturation.

Our current study unanticipatedly found that Pds5A distributes on the spindle microtubules to coordinate the spindle building during oocyte meiotic maturation, thereby ensuring chromosome euploidy, oocyte meiotic progression, and animal fertility. These unique functions of Pds5 proteins in oocytes are independent of their canonical roles in chromosome cohesion during mitotic cell cycle. In particular, we observed that Pds5 depletion in oocytes primarily causes short spindles, which further activates SAC to arrest oocytes

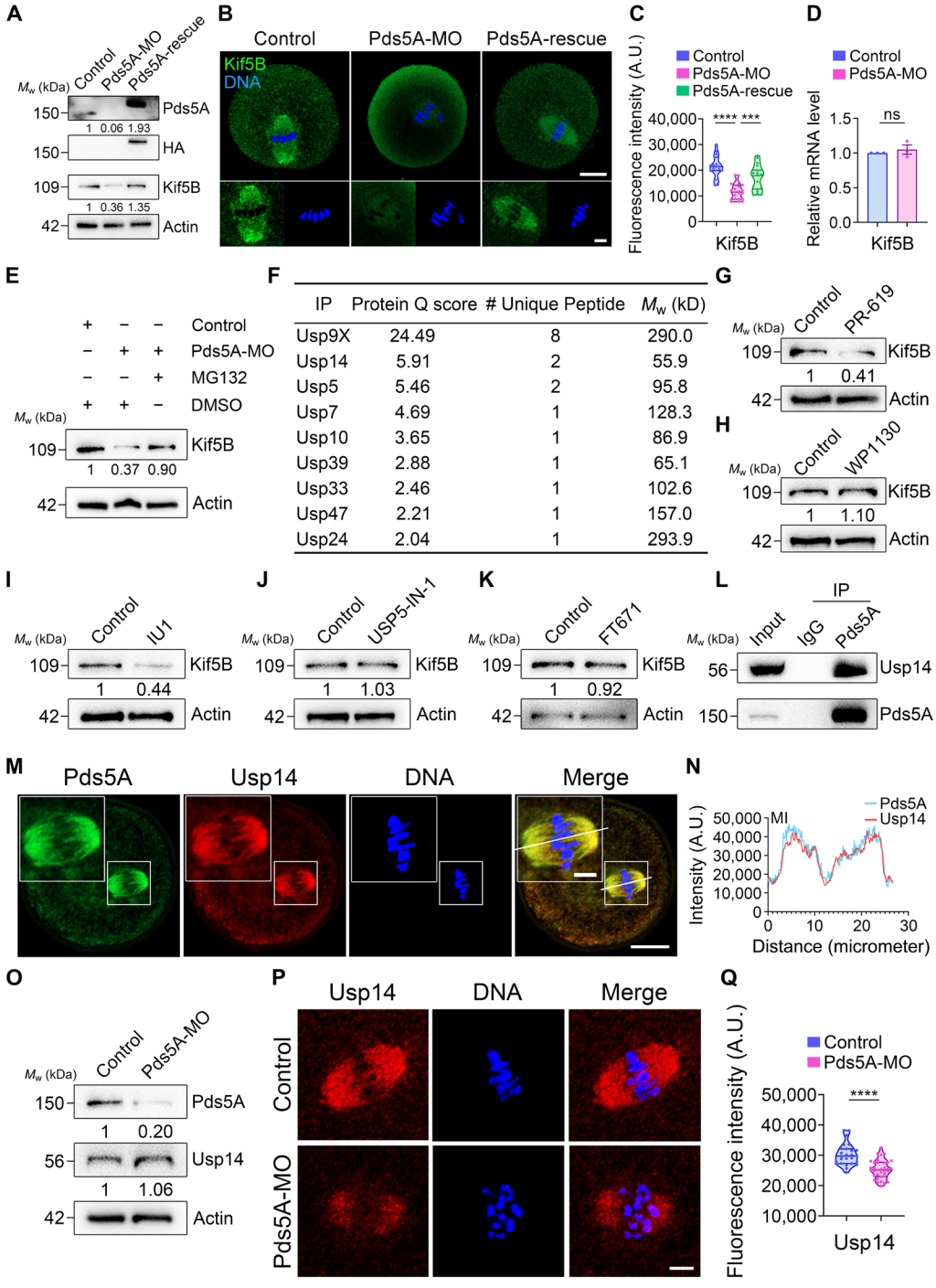

Fig. 7. Recruitment of Usp14 by Pds5A stabilizes Kif5B in mouse oocytes. (**A**) Immunoblotting analysis showing the protein levels of Kif5B in control, Pds5A-MO, and Pds5A-rescue oocytes. (**B**) Fluorescence images of Kif5B in control, Pds5A-MO, and Pds5A-rescue oocytes at MI stage. Scale bars, 20 and 5 μm. (**C**) The fluorescence intensity of Kif5B signals in control ($n = 19$), Pds5A-MO ($n = 20$), and Pds5A-rescue ($n = 19$) oocytes at MI stage. (**D**) qRT-PCR analysis showing the mRNA levels of Kif5B in control ($n = 30$) and Pds5A-MO ($n = 30$) oocytes. (**E**) Immunoblotting analysis showing the protein levels of Kif5B in control, Pds5A-MO, and Pds5A-MO+MG132 (10 μM) oocytes. (**F**) Representative binding DUBs of Pds5A as shown in MS data. (**G** to **K**) Immunoblotting analysis showing the protein levels of Kif5B in control, PR-619-treated, WP1130-treated, IU1-treated, USP5-IN-1-treated, and FT671-treated oocytes, respectively. PR-619 (10 μM), 10 μM WP1130, 25 μM IU1, 10 μM USP5-IN-1, and 10 μM FT671 were used to treat GV oocytes for 22 hours, respectively. (**L**) Co-IP of Pds5A and Usp14 as precipitated with Pds5A antibody. (**M**) Costaining of Pds5A and Usp14 in oocytes at MI stage. Scale bars, 20 and 5 μm. (**N**) Fluorescence intensity profiles of Pds5A and Usp14 along the white line in (M). (**O**) Immunoblotting analysis showing the protein levels of Usp14 in control and Pds5A-MO oocytes. (**P**) Fluorescence images of Usp14 in control and Pds5A-MO oocytes at MI stage. Scale bar, 5 μm. (**Q**) The fluorescence intensity of Usp14 signals in control ($n = 26$) and Pds5A-MO ($n = 35$) oocytes at MI stage. Data in (D) were designated as mean percentage (means ± SEM), and (C) and (Q) were designated as mean value (means ± SD) of at least three independent experiments. ***$P < 0.001$; ****$P < 0.0001$; ns, no significance.

at MI stage. Certainly, other aberrant spindle types such as elongated or pole-defective morphology can also result in SAC activation and oocyte MI arrest (*26*). The meiotic role of Pds5 proteins has been previously reported in yeast and male mouse. Pds5 interacts with proteasomes to regulate meiotic chromosome axis length by modulating ubiquitination in budding yeast (*24*). In mouse spermatocytes, Pds5A and Pds5B exert redundant functions in completion of meiotic prophase I via regulating the length of axial elements and telomere integrity (*18*). Notably, Pds5A is present at the axial/lateral elements of the synaptonemal complex by zygotene and found at centromeric domains in both MI and MII spermatocytes (*18*). In contrast, we did not observe the centromeric localization of Pds5A in mouse oocytes, indicating that Pds5A might play distinct roles in male and female meiosis.

We further carried out co-IP coupled with MS to uncover the potential molecular mechanisms underlying the involvement of Pds5A in the meiotic spindle assembly and found that Pds5A interacted with Kif5B on the spindle apparatus. Although Kif5B has been implicated in the microtubule dynamics and spindle organization in mitotic cells and is required for PBE in mouse oocytes (*28*, *29*, *33*), whether Kif5B participates in the meiotic spindle assembly in oocytes is unclear. We then evidenced the requirement of Kif5B during spindle organization in oocytes and validated that expression of Kif5B mitigated the meiotic defects caused by Pds5A depletion, indicating that Pds5A acts on the spindle assembly through Kif5B. On the other hand, it also suggests that the spindle localization of Kif5B might not be dependent on Pds5A. Otherwise, exogenous Kif5B cannot be located to the spindle apparatus to restore the spindle assembly in Pds5-depleted oocytes.

Another important finding in our study is that we elucidated how Pds5A regulated protein levels of its downstream effector Kif5B. From MS data of Pds5A, we noticed that many DUBs were present as its potential binding partners. DUBs are a class of proteases that cleave ubiquitin attached to substrates or within ubiquitin chains to regulate protein stability and thus extensively take part in many biological processes (*34*). By pharmacological inhibition screening, we identified that Usp14 was responsible for the protein stability of Kif5B. Usp14 is engaged in various signaling pathways, correlating with neurodegenerative disease, immune response, autophagy, and cancer (*35*). We here unveiled that Usp14 accumulated on the spindle in oocytes, and this localization pattern was regulated by Pds5A.

To sum up, on the basis of our investigations, we propose a model that during oocyte meiotic maturation, Pds5A is located on the spindle apparatus to form a scaffold platform for docking and bridging Kif5B and Usp14 to control the spindle elongation. Loss of function of Pds5A results in spindle abnormality-induced oocyte maturation arrest or aneuploidy, and thereby impairing the female fertility (fig. S11). Our findings reveal that the cohesin-associated protein can be used as a spindle regulator to orchestrate meiotic cell cycle in female germ cells.

MATERIALS AND METHODS

Animals

Four- to six-week-old female ICR mice were maintained under controlled conditions of temperature (20° to 23°C) and light (12-hour light-dark cycle) with free access to food and water throughout the study. All mouse protocols and experimental procedures were approved by the Animal Research Institute Committee of Nanjing Agricultural University, China.

Generation of knockout mice

Pds5A$^{+/-}$ mice were obtained from GemPharmatech (Nanjing, China) and generated by CRISPR-Cas9 technology.

Antibodies and reagents

Rabbit polyclonal anti-Pds5A antibodies were purchased from Proteintech (Rosemont, IL, USA; catalog no.: 17485-1-AP) and Bethyl Laboratories (Montgomery, TX, USA; catalog no.: A300-089A-T); mouse monoclonal anti-Pds5A antibody was purchased from Santa Cruz Biotechnology (Dallas, Texas, USA; catalog no.: sc-515263); mouse monoclonal anti–α-tubulin–fluorescein isothiocyanate (FITC) antibody was purchased from Sigma-Aldrich (St. Louis, MO, USA; catalog no.: F2168); sheep polyclonal anti-BubR1 antibody was purchased from Abcam (Cambridge, MA, USA; catalog no.: ab28193); rabbit polyclonal anti-Mad2L1 antibody was purchased from Proteintech (catalog no.: 10337-1-AP); human anti-centromere antibody was purchased from Antibodies Incorporated (Davis, CA, USA; catalog no.: CA95617); rabbit polyclonal anti-Kif5B antibody was purchased from ABclonal Technology (Wuhan, China; catalog no.: A15284); mouse monoclonal anti-Kif5B antibody was purchased from Santa Cruz Biotechnology (catalog no.: sc-133184); mouse monoclonal anti–β-actin antibody was purchased from Proteintech (catalog no.: 60008-1-Ig); mouse monoclonal anti-Usp14 antibody was purchased from Santa Cruz Biotechnology (catalog no.: sc-398009); rabbit polyclonal anti-Usp14 antibody was purchased from Proteintech (catalog no.: 14517-1-AP); rabbit monoclonal anti-Rec8 antibody was purchased from Abcam (catalog no.: ab192241); mouse monoclonal anti-Rad21 antibody was purchased from Sigma-Aldrich (catalog no.: 05-908); rabbit polyclonal anti-HA antibody was purchased from Proteintech (catalog no.: 51064-2-AP); rabbit monoclonal anti-Myc antibody was purchased from ABclonal Technology (catalog no.: AE070).

3-isobutyl-1-metyl-xanthine (IBMX) was purchased from Sigma-Aldrich (catalog no.: I5879); MG132 was purchased from Selleckchem (Houston, Texas, USA; catalog no.: S2619); PR-619 was purchased from MedChemExpress (New Jersey, USA; catalog no.: HY-13814); WP1130 was purchased from MedChemExpress (catalog no.: HY-13264); IU1 was purchased from MedChemExpress (catalog no.: HY-13817); Usp5-IN-1 was purchased from MedChemExpress (catalog no.: HY-139979); FT671 was purchased from MedChemExpress (catalog no.: HY-107985); Reversine was purchased from MedChemExpress (catalog no.: HY-14711).

Mouse oocyte collection and maturation

As previously described (*36*), fully grown oocytes arrested at GV stage were collected from the ovaries of female ICR mice in M2 medium and then cultured in M16 medium under liquid paraffin oil at 37°C in an atmosphere of 5% CO_2 incubator for in vitro maturation. At different time points after culture, oocytes were collected for subsequent analysis.

MO and siRNA knockdown

As previously described (*36*), Pds5A-targeting MO antisense oligo (Gene Tools, Philomath, OR, USA; 5′-CTTCGGCTGCGTGAAGTCCATCCTG-3′) was diluted with water to provide a working concentration of 1 mM, and then approximately 5 to 10 pl of oligos was microinjected into the cytoplasm of fully grown mouse GV oocytes using a Narishige microinjector (Tokyo, Japan). A nontargeting MO oligo (5′-CCTCTTACCTCAGTTACAATTTATA-3′) was

injected as a control. To facilitate MO-mediated inhibition of mRNA translation, oocytes were arrested at GV stage in M16 medium containing 100 μM IBMX for 20 hours and then cultured in IBMX-free M16 medium for further experiments.

Pds5A-targeting siRNA oligo (Santa Cruz Biotechnology, sc152143), Kif5B-targeting siRNA oligos (GenePharma, Shanghai, China; antisense sequences: 5′-UAUUGUUCCAUUAUAGCCCTT-3′, 5′-AUUAUCGCGUACCAACUGCTT-3′, 5′-AUAAUUAACAGCCAGUUCCTT-3′), or Usp14-targeting siRNA oligo (GenePharma; antisense sequence: 5′-AAGAAUCCGUCUCUCUACCTT-3′) were diluted with water to provide a working concentration of 20 μM, and then approximately 5 to 10 pl of oligos was microinjected into the cytoplasm of fully grown mouse GV oocytes using a Narishige microinjector. A nontargeting siRNA oligo (Santa Cruz Biotechnology, sc-37007) was injected as a control. To facilitate the degradation of mRNA by siRNA, mouse oocytes were arrested at GV stage in M16 medium containing 100 μM IBMX for 20 hours and then transferred to IBMX-free M16 medium to resume the meiosis for subsequent experiments (*36*).

Knockdown of Pds5A in porcine oocytes was achieved via microinjection of 25 μM Pds5A-targeting siRNA oligos (GenePharma; antisense sequences: 5′-UAAAGGGUUAUGAAGAGGCTT-3′, 5′-UUUAUGUCCUCAAACCCACTT-3′, 5′-UAACAUAGAAAUGUGGCCCTT-3′). A nontargeting siRNA oligo (antisense sequence: 5′-ACGUGACACGUUCGGAGAATT-3′) was injected as a control. Porcine oocytes were arrested at GV stage in TCM-199 medium containing 100 μM IBMX for 24 hours and then transferred to IBMX-free TCM-199 medium to resume the meiosis for further experiments (*36*).

mRNA construct and in vitro transcription

Pds5A cDNA was subcloned into pcDNA3.1/6×HA vector. Kif5B cDNA was subcloned into pCS2/6×Myc vector. As previously described (*37*), capped mRNA was synthesized from linearized plasmid using T7 or SP6 mMessage mMachine kit (Thermo Fisher Scientific, Waltham, MA, USA) and purified with MEGAclear kit (Thermo Fisher Scientific). Typically, 10 to 12 pl of 0.5 to 1.0 μg/μl mRNA was injected into oocytes and then arrested at GV stage in M16 medium containing 100 μM IBMX for 4 hours, allowing enough time for translation, followed by releasing into IBMX-free M16 medium for further study.

Immunofluorescence staining and confocal microscopy

Oocytes were fixed in 4% paraformaldehyde in phosphate-buffered saline (PBS) (pH 7.4) for 30 min and permeabilized in 0.5% Triton X-100 for 20 min (mouse oocytes) or 1% Triton X-100 for 1 hour (porcine oocytes) at room temperature. Oocytes were then blocked with 1% bovine serum albumin–supplemented PBS for 1 hour and incubated with the appropriate primary antibodies [Pds5A (1:50), α-tubulin–FITC (1:300), CREST (1:200), BubR1 (1:100), Mad2L1 (1:100), Rec8 (1:50), Rad21 (1:50), Kif5B (1:50), Usp14 (1:50), HA (1:100), or Myc (1:100)] at 4°C overnight. After washing in PBST, the oocytes were incubated with a corresponding secondary antibody for 1 hour at room temperature and then counterstained with Hoechst 33342 (10 μg/ml) for 10 min. Lastly, oocytes were mounted on glass slides and imaged by laser confocal microscope (LSM 900, Carl Zeiss, Germany). The quantification of fluorescence intensity was performed as we described previously (*36*).

Chromosome spreading and kinetochore staining

As previously described (*36*), oocytes were incubated in Tyrode's buffer (pH 2.5) for about 30 s at 37°C to remove zona pellucidae. After recovery in M2 medium for 10 min, the oocytes were fixed in a drop of 1% paraformaldehyde with 0.15% Triton X-100 on a glass slide. After air drying, the oocytes were incubated with CREST antibody (1:200) at 4°C overnight and then probed with Alexa Fluor 555–conjugated secondary antibody for 1 hour for kinetochore staining. Chromosomes were then counterstained with Hoechst 33342 and examined by confocal microscopy.

Immunoprecipitation and immunoblotting

Immunoprecipitation was carried out using 20 mouse ovaries according to the instruction for ProFound Mammalian CoImmunoprecipitation Kit (Thermo Fisher Scientific). For immunoblotting, as previously described (*37*), 150 to 300 oocytes were lysed in 4 × LDS sample buffer (Thermo Fisher Scientific) containing protease inhibitor and then separated on 10% bis-tris precast gels and transferred onto polyvinylidene difluoride membranes. The blots were blocked in TBST containing 5% low-fat dry milk for 1 hour at room temperature and then incubated with anti-Pds5A (1:1000), anti-Kif5B (1:500), anti-Usp14 (1:2000), anti-HA (1:4000), or anti–β-actin (1:5000) antibodies overnight at 4°C. After three times of wash in TBST, the blots were incubated with horseradish peroxidase–conjugated secondary antibodies for 1 hour at room temperature. Chemiluminescence signals were detected with ECL Plus (Thermo Fisher Scientific), and protein bands were acquired by Tanon-3900 Chemiluminescence Imaging System (Tanon, Beijing, China). Band intensities were quantified using ImageJ software and normalized to loading controls.

Liquid chromatography tandem MS and data analysis

The dried peptide samples were reconstituted with mobile phase A [2% acetonitrile (ACN) and 0.1% formic acid (FA)], centrifuged at 20,000*g* for 10 min, and the supernatant was taken for injection. Separation was performed by Thermo UltiMate 3000 UHPLC. The sample was first enriched in trap column and desalted, then placed in a self-packed C18 column (75-μm internal diameter, 3-μm column size, and 25-cm column length), and separated at a flow rate of 300 nl/min by the following effective gradient: 0 ~ 5 min, 5% mobile phase B (98% ACN and 0.1% FA); 5 ~ 45 min, mobile phase B linearly increased from 5 to 25%; 45 ~ 50 min, mobile phase B increased from 25 to 35%; 50 ~ 52 min, mobile phase B rose from 35 to 80%; 52 ~ 54 min, 80% mobile phase B; 54 ~ 60 min, 5% mobile phase B. The peptides separated by liquid-phase chromatography were ionized by a nanoESI source and then passed to a tandem mass spectrometer Q-Exactive HF X (Thermo Fisher Scientific) for DDA (data-dependent acquisition) mode detection.

Protein identification was achieved by searching the obtained MS spectra files using software Mascot Software (Mascot v2.3.02) against a database from UniProt mouse protein sequencing data. Results from search engine were preprocessed and rescored using Percolator to improve the matching accuracy. The output was then filtered by false discovery rate (FDR) 1% at spectral level (PSM-level FDR ≤ 0.01) to obtain a significant identified spectrum and peptide list.

RNA isolation and quantitative real-time PCR

Total RNA was extracted from a total of 30 oocytes using Dynabeads mRNA DIRECT Kit (Thermo Fisher Scientific) and then

reversed to cDNA and stored at −20°C until use. Gene expression was determined by quantitative real-time PCR using a ChamQ SYBR qPCR Master Mix (Vazyme, Nanjing, China). Each PCR reaction consisted of 10 μl of 2 × ChamQ SYBR qPCR Master Mix, 7 μl of water, 2 μl of cDNA sample, and 1 μl of gene-specific primers, and run in a Light Cycler instrument (Thermo Fisher Scientific).

Fertility test

WT or *Pds5A*$^{+/-}$ females were co-caged with WT males of proven fertility to determine the number and size of litters for a period of 4 to 6 months.

Porcine oocyte collection and in vitro maturation

The procedures for porcine oocyte collection and in vitro maturation were performed as we described previously (*38*).

Statistical analysis

As previously described (*36*), all statistical data from at least three independent experiments were presented as means ± SEM or SD unless otherwise stated, and the number of samples used in each group was labeled in parentheses as (*n*). Data were analyzed by two-tailed unpaired *t* test, which is provided by GraphPad Prism 8 statistical software. $P < 0.05$ was considered as statistical significance.

Supplementary Materials

The PDF file includes:

Figs. S1 to S11
Table S1
Legend for dataset S1

Other Supplementary Material for this manuscript includes the following:

Dataset S1

REFERENCES AND NOTES

1. B. Xiong, J. L. Gerton, Regulators of the cohesin network. *Annu. Rev. Biochem.* **79**, 131–153 (2010).
2. V. Makrantoni, A. L. Marston, Cohesin and chromosome segregation. *Curr. Biol.* **28**, R688–R693 (2018).
3. K.-i. Ishiguro, Y. Watanabe, Chromosome cohesion in mitosis and meiosis. *J. Cell Sci.* **120**, 367–369 (2007).
4. T. Hirano, Chromosome cohesion, condensation, and separation. *Annu. Rev. Biochem.* **69**, 115–144 (2000).
5. J.-M. Peters, A. Tedeschi, J. Schmitz, The cohesin complex and its roles in chromosome biology. *Genes Dev.* **22**, 3089–3114 (2008).
6. R. V. Skibbens, Establishment of sister chromatid cohesion. *Curr. Biol.* **19**, R1126–R1132 (2009).
7. N. Zhang, L. E. Coutinho, D. Pati, PDS5A and PDS5B in cohesin function and human disease. *Int. J. Mol. Sci.* **22**, 5868 (2021).
8. T. Nishiyama, M. M. Sykora, P. J. Huis in 't Veld, K. Mechtler, J.-M. Peters, Aurora B and Cdk1 mediate Wapl activation and release of acetylated cohesin from chromosomes by phosphorylating sororin. *Proc. Natl. Acad. Sci. U.S.A.* **110**, 13404–13409 (2013).
9. Z. Ouyang, G. Zheng, D. R. Tomchick, X. Luo, H. Yu, Structural basis and IP6 requirement for Pds5-dependent cohesin dynamics. *Mol. Cell* **62**, 248–259 (2016).
10. A. F. Neuwald, T. Hirano, HEAT repeats associated with condensins, cohesins, and other complexes involved in chromosome-related functions. *Genome Res.* **10**, 1445–1452 (2000).
11. S. Panizza, T. Tanaka, A. Hochwagen, F. Eisenhaber, K. Nasmyth, Pds5 cooperates with cohesin in maintaining sister chromatid cohesion. *Curr. Biol.* **10**, 1557–1564 (2000).
12. K. Choudhary, Z. Itzkovich, E. Alonso-Perez, H. Bishara, B. Dunn, G. Sherlock, M. Kupiec, S. cerevisiae cells can grow without the Pds5 cohesin subunit. *MBio* **13**, e0142022 (2022).
13. Z. Ouyang, H. Yu, Releasing the cohesin ring: A rigid scaffold model for opening the DNA exit gate by Pds5 and Wapl. *Bioessays* **39**, 1600207 (2017).
14. N. Al-Jomah, L. Mukololo, A. Anjum, M. Al Madadha, R. Patel, Pds5A and Pds5B display non-redundant functions in mitosis and their loss triggers Chk1 activation. *Front. Cell Dev. Biol.* **8**, 531 (2020).
15. N. L. Arruda, A. F. Bryan, J. M. Dowen, PDS5A and PDS5B differentially affect gene expression without altering cohesin localization across the genome. *Epigenetics Chromatin* **15**, 30 (2022).
16. C. Morales, M. Ruiz-Torres, S. Rodriguez-Acebes, V. Lafarga, M. Rodriguez-Corsino, D. Megías, D. A. Cisneros, J.-M. Peters, J. Méndez, A. Losada, PDS5 proteins are required for proper cohesin dynamics and participate in replication fork protection. *J. Biol. Chem.* **295**, 146–157 (2020).
17. D. Yu, G. Chen, Y. Wang, Y. Wang, R. Lin, N. Liu, P. Zhu, H. Liu, T. Hu, R. Feng, H. Feng, F. Lan, J. Cai, H. Chen, Regulation of cohesin-mediated chromosome folding by PDS5 in mammals. *EMBO Rep.* **23**, e54853 (2022).
18. A. Viera, I. Berenguer, M. Ruiz-Torres, R. Gómez, A. Guajardo, J. L. Barbero, A. Losada, J. A. Suja, PDS5 proteins regulate the length of axial elements and telomere integrity during male mouse meiosis. *EMBO Rep.* **21**, e49273 (2020).
19. J. Gao, Y. Qin, J. C. Schimenti, Gene regulation during meiosis. *Trends Genet.* **40**, 326–336 (2024).
20. H. Ohkura, Meiosis: An overview of key differences from mitosis. *Cold Spring Harb. Perspect. Biol.* **7**, a015859 (2015).
21. H. Jin, V. Guacci, H.-G. Yu, Pds5 is required for homologue pairing and inhibits synapsis of sister chromatids during yeast meiosis. *J. Cell Biol.* **186**, 713–725 (2009).
22. D.-Q. Ding, N. Sakurai, Y. Katou, T. Itoh, K. Shirahige, T. Haraguchi, Y. Hiraoka, Meiotic cohesins modulate chromosome compaction during meiotic prophase in fission yeast. *J. Cell Biol.* **174**, 499–508 (2006).
23. M. Song, B. Zhai, X. Yang, T. Tan, Y. Wang, X. Yang, Y. Tan, T. Chu, Y. Cao, Y. Song, S. Wang, L. Zhang, Interplay between Pds5 and Rec8 in regulating chromosome axis length and crossover frequency. *Sci. Adv.* **7**, eabe7920 (2021).
24. X. Yang, M. Song, Y. Wang, T. Tan, Z. Tian, B. Zhai, X. Yang, Y. Tan, Y. Cao, S. Dai, S. Wang, L. Zhang, The ubiquitin-proteasome system regulates meiotic chromosome organization. *Proc. Natl. Acad. Sci. U.S.A.* **119**, e2106902119 (2022).
25. S. Zhu, P. Xie, Y. Yang, Y. Wang, C. Zhang, Y. Zhang, S. Si, J. Zhang, J. He, H. Si, K. Fang, B. Ma, X. Jiang, L. Huang, J. Li, T. Min, B. Zheng, L. Da, D. Lin, K. Gao, Y. Li, M. Huang, F. Qiao, H. Huo, H. Feng, H. Zhao, Z. Chen, Z. Xu, J. Xie, H. Cao, J. Liu, X. Yao, W. Xie, Y. Sun, K. Wu, B. Xiong, P. Hu, Z. Luo, C. Lin, Maternal ELL3 loss-of-function leads to oocyte aneuploidy and early miscarriage. *Nat. Struct. Mol. Biol.* **32**, 381–392 (2025).
26. Z.-0. Y. Xu, X.-S. Ma, S.-T. Qi, Z.-B. Wang, L. Guo, H. Schatten, Q.-Y. Sun, Y.-P. Sun, Cep55 regulates spindle organization and cell cycle progression in meiotic oocyte. *Sci. Rep.* **5**, 16978 (2015).
27. B. Zhang, J. Chang, M. Fu, J. Huang, R. Kashyap, E. Salavaggione, S. Jain, S. Kulkarni, M. A. Deardorff, M. L. G. Uzielli, D. Dorsett, D. C. Beebe, P. Y. Jay, R. O. Heuckeroth, I. Krantz, J. Milbrandt, Dosage effects of cohesin regulatory factor PDS5 on mammalian development: Implications for cohesinopathies. *PLOS ONE* **4**, e5232 (2009).
28. V. Daire, J. Giustiniani, I. Leroy-Gori, M. Quesnoit, S. Drevensek, A. Dimitrov, F. Perez, C. Poüs, Kinesin-1 regulates microtubule dynamics via a c-Jun N-terminal kinase-dependent mechanism. *J. Biol. Chem.* **284**, 31992–32001 (2009).
29. H. Gan, W. Xue, Y. Gao, G. Zhu, D. Chan, K. S. E. Cheah, J. Huang, KIF5B modulates central spindle organization in late-stage cytokinesis in chondrocytes. *Cell Biosci.* **9**, 85 (2019).
30. C. Perea-Resa, L. Wattendorf, S. Marzouk, M. D. Blower, Cohesin: Behind dynamic genome topology and gene expression reprogramming. *Trends Cell Biol.* **31**, 760–773 (2021).
31. J. R. Sanders, K. T. Jones, Regulation of the meiotic divisions of mammalian oocytes and eggs. *Biochem. Soc. Trans.* **46**, 797–806 (2018).
32. N. R. Kudo, K. Wassmann, M. Anger, M. Schuh, K. G. Wirth, H. Xu, W. Helmhart, H. Kudo, M. M. Kay, B. Maro, J. Ellenberg, P. de Boer, K. Nasmyth, Resolution of chiasmata in oocytes requires separase-mediated proteolysis. *Cell* **126**, 135–146 (2006).
33. D. Kidane, D. Sakkas, T. Nottoli, J. McGrath, J. B. Sweasy, Kinesin 5B (KIF5B) is required for progression through female meiosis and proper chromosomal segregation in mitotic cells. *PLOS ONE* **8**, e58585 (2013).
34. S. M. Lange, L. A. Armstrong, Y. Kulathu, Deubiquitinases: From mechanisms to their inhibition by small molecules. *Mol. Cell* **82**, 15–29 (2022).
35. F. Wang, S. Ning, B. Yu, Y. Wang, USP14: Structure, function, and target Inhibition. *Front. Pharmacol.* **12**, 801328 (2021).
36. C. Zhou, Y. Miao, Z. Cui, X. ShiYang, Y. Zhang, B. Xiong, The cohesin release factor Wapl interacts with Bub3 to govern SAC activity in female meiosis I. *Sci. Adv.* **6**, eaax3969 (2020).
37. Y. Miao, P. Wang, B. Xie, M. Yang, S. Li, Z. Cui, Y. Fan, M. Li, B. Xiong, BRCA2 deficiency is a potential driver for human primary ovarian insufficiency. *Cell Death Dis.* **10**, 474 (2019).
38. Y. Miao, Z. Cui, X. Zhu, Q. Gao, B. Xiong, Supplementation of nicotinamide mononucleotide improves the quality of postovulatory aged porcine oocytes. *J. Mol. Cell Biol.* **14**, mjac025 (2022).

Acknowledgments

Funding: This work was supported by the Zhejiang Provincial Natural Science Foundation (LZ25C170003 to B.X.) and the National Key Research and Development Program of China (2023YFD1300502 to B.X.). **Author contributions:** Conceptualization: B.X. and Y.Z. Investigation: Y.Z. and J.B. Validation: Y.Z. and J.B. Data curation: Y.Z. and J.B. Formal analysis: Y.Z. and J.B. Resources: Y.Z. Visualization: Y.Z. Supervision: B.X. Project administration: B.X.

Funding acquisition: B.X. Writing—original draft: Y.Z. and J.B. Writing—review and editing: B.X. **Competing interests:** The authors declare that they have no competing interests. **Data and materials availability:** All data needed to evaluate the conclusions in the paper are present in the paper and/or the Supplementary Information.

Submitted 3 October 2024
Accepted 6 March 2025
Published 11 April 2025
10.1126/sciadv.adt6159